

FEM-based Estimation of Reactivity Change due to Core Deformation in SFR

Woong Heo and Yonghee Kim*

Korea Advanced Institute of Science and Technology: 291 Daehak-ro, Yuseong-gu, Daejeon, South Korea, 34141

*Corresponding author: yongheekim@kaist.ac.kr

Abstract - In sodium-cooled fast reactors, the fuel assembly deformation due to thermo-mechanical effects, irradiation, and structural restrictions results in very tangled behaviors. Reactivity feedback caused by this deformation or distortion of the assembly is a key parameter in the inherent safety analysis of fast reactor systems. However, to date, there has been no accurate and efficient deterministic way to compute directly the reactivity change caused by actual local perturbations. To overcome this difficulty, the multi-group diffusion equations are solved by the Galerkin finite element method (FEM) with linear shape functions to directly estimate the reactivity change due to local core deformations in sodium-cooled fast reactors. Assessment of reactivity changes were conducted for 5 types of deformation scenarios, and it is shown that diffusion analysis based on FEM with linear shape functions can properly estimate the reactivity change by geometric perturbation in fast reactors with less than ~2.5 pcm error.

I. INTRODUCTION

The sodium-cooled fast reactor (SFR) is promising in terms of Gen-IV reactor design with advantages in the utilization of uranium resources and the low production and potential transmutation of radioactive wastes. Complicated deformation of fuel assemblies in a fast reactor is well-known phenomenon. One dominant and important source of reactivity feedback is the geometric distortion that is composed of bowing, expansion and swelling caused by thermo-mechanical effects and irradiation. Negative reactivity feedback caused by the geometric distortion in fast reactors is a key parameter for inherent safety for these advanced reactors [1].

However, it is not easy to evaluate the reactivity change accurately because the geometric distortion is a very tangled and complicated behavior which is affected by thermo-mechanical and irradiation effects simultaneously, even including external sources (i.e., restraint rings or load pads). In the thermal point of view, thermal gradients bring on the localized thermal expansions of assemblies and core structures during normal operation and transients in fast reactors. Unfortunately, this kind of localized deformations have not been widely studied in the neutronics field, resulting in a lack of generic, accurate, and efficient way to compute the reactivity changes caused by the local perturbations and events.

The conventional way to estimate the reactivity feedback caused by geometry distortions is limited to uniform swelling or expansion cases, and it does not account for irregular local changes. Although accurate geometric deformations and associated reactivity changes can be analyzed by using the Monte Carlo method, but it requires lots of computational power to estimate even a single reactivity change and the statistical error makes it difficult to estimate a small reactivity change.

To surmount this difficulty, many methods based on perturbation theory have been proposed, and recently, so-

called "Virtual Density" theory was suggested and has shown accurate reactivity estimation for both uniform and non-uniform swellings [2]. Even though the effect of geometry distortion in fast reactors has long been acknowledged, impacts of actual displacements or local deformations of fuel assemblies have not been properly estimated. Reactivity perturbation by the geometric deformations in SFRs is also considered to be an important design and safety topic during many transient scenarios.

The main purpose of this study is to develop a computer code which can evaluate the deformation-related reactivity changes by directly modelling local deformations of fuel assemblies in SFRs. In order to consider the localized deformation and to maximize computational efficiency, multi-group diffusion equation based on Galerkin finite element method (FEM) is adopted for an SFR analysis. In this study, 2-D core calculations with unstructured triangular elements were conducted as a bridgehead before the estimation of reactivity changes in 3-D. A linear approximation was used for the shape function in FEM because another objective of this study is to verify the feasibility of utilizing low-order approximations for the estimation of reactivity changes due to core deformation in SFR.

II. REACTIVITY ESTIMATION WITH ASSEMBLY DEFORMATION

A 2-D multi-group diffusion equation solver based on FEM with a simple triangular mesh and linear shape function was developed for fast reactor analysis in this study. A 2-D homogeneous Proto-type Gen-IV Sodium-cooled Fast Reactor (PGSFR) is chosen as the reference core model and is shown in Fig. 1 [3]. A total of ten junction points between hexagonal assemblies were selected as geometric perturbation spots to imitate the irregular distortion of assemblies in the fast reactor. The directions of the node movement for geometric perturbation are also depicted in

Fig. 1 as arrows. In this study, regular core expansion cases were simulated in addition to irregular deformations to verify the main arguments.

The 9-group constants were generated by using the TRANSX/TWODANT code system which was conventionally used for group constant generation [4, 5]. For simplicity, it is assumed that microscopic cross sections and fission spectrum χ_g are not changed after expansion or shrinkage of assemblies in the core because they are usually unaffected by small changes in a fast reactor except for extreme cases. Therefore, only the atomic number densities of the deformed hexagon assemblies were modified to compensate for the change of macroscopic cross sections in accordance with a volume ratio as shown in Eq. (1).

$$\frac{V_{original}}{V_{perturbed}} = W_{ND} \quad (1)$$

$$N_{perturbed} = W_{ND} \times N_{original}$$

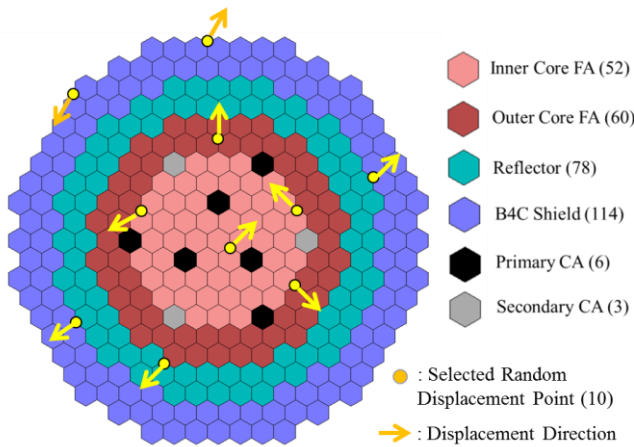


Fig. 1. Radial Core Configuration of PGSFR

From the Eq. (1), three types of 9-group macroscopic cross sections are plotted (nu-fission, absorption, and diffusion coefficient) with respect to volume ratio in the range of 0.8~1.2. As shown in Fig. 2 and 3, nu-fission and absorption cross sections are proportional to volume ratio, also clearly shown in Eq. (1). In contrast, diffusion coefficients decrease as the volume ratio increases as shown in Fig. 4. This is because the diffusion coefficient is inversely proportional to the total or transport cross sections.

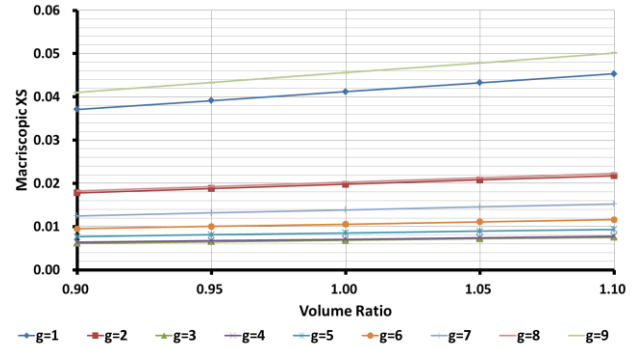


Fig. 2. 9-group nu-fission XS vs. Volume Ratio (Inner Core FA)

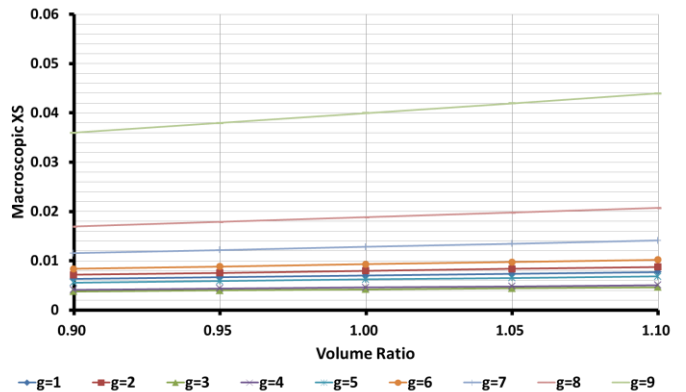


Fig. 3. 9-group Absorption XS vs. Volume Ratio (Inner Core FA)

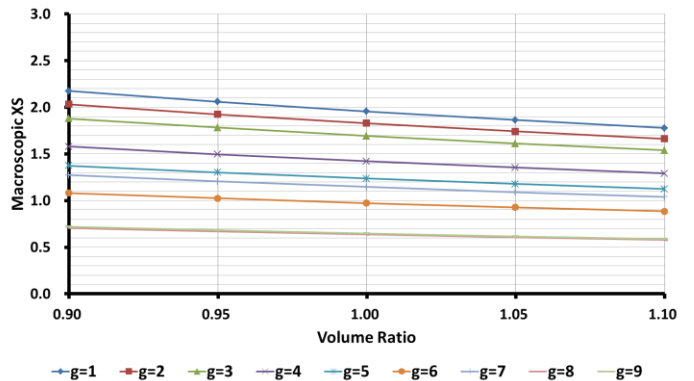


Fig. 4. 9-group Diffusion Coefficient vs. Volume Ratio (Inner Core FA)

Eventually, reactivity changes calculated by the diffusion equation solver based on FEM were compared to the results which were calculated by using MCNP5 [6]. The exactly same 9-group constants and geometries (before and after perturbation) were used for both FEM and MCNP5 calculations.

1. Finite Element Method for Multi-group Diffusion Equation with unstructured triangular element

The 2-D multi-group diffusion equation without an external neutron source is given in Eq. (2).

$$-\nabla \cdot D_g \nabla \phi_g + \Sigma_{rg} \phi_g = \sum_{g'=1}^{G, g' \neq g} (\Sigma_{sg' \rightarrow g} \phi_{g'}) + \frac{1}{k_{eff}} \chi_g \sum_{g'=1}^G (\nu \Sigma_{fg'} \phi_{g'}) \quad (2)$$

$$\phi_g(x, y) = \sum_{e=1}^E \left[\phi_{g,i} \eta_i^e(x, y) + \phi_{g,j} \eta_j^e(x, y) + \phi_{g,k} \eta_k^e(x, y) \right] \quad (3)$$

By using the Galerkin method and linear shape function for flux as shown in Eq. (3), the final form of Eq. (2) can be expressed as Eq. (4).

$$\sum_{e=1}^E \left[\int_{D_e} D_{g,e} \nabla \eta_j \cdot \nabla \eta_i + \Sigma_{rg,e} \eta_j \eta_i d\Omega + \int_{\Gamma_e} \gamma \eta_j \eta_i dS \right] = \sum_{e=1}^E \left\{ \begin{array}{l} \left(\sum_{g'=1}^{G, g' \neq g} (\Sigma_{sg' \rightarrow g, e} \int_{D_e} \eta_j \eta_i d\Omega) \right) \phi_{g',i} \\ + \frac{1}{k_{eff}} \sum_{g'=1}^G (\chi_{g,e} (\nu_{g'} \Sigma_{fg', e} \int_{D_e} \eta_j \eta_i d\Omega) \phi_{g',i} \end{array} \right\} \quad (4)$$

It is possible to generate each component in group-wise neutron loss and production matrices (LHS and RHS terms, respectively) from the Eq. (4) by the combination of node indices in each element. The implemented solver code can generate the problem matrices and calculate the final solution for fast reactor analysis. The solver code takes any absolute positions for each node in a problem domain so that any type of triangle element can be applicable. This is for accommodating to any irregular deformation of assemblies.

To provide the node and element information to the solver, an independent mesh generator was also developed. The mesh generator can produce a structured triangular mesh grid as a basic uniform triangulation for each hexagon assembly in a reactor model. An additional function is that a bundle of nodes in the structured triangular mesh grid can be moved depending on movements at the 6 vertices of hexagon assembly as shown in Fig. 5.

2. Regular and Irregular Assembly Deformation

As a preliminary verification, reactivity changes due to the regular uniform expansion of all assemblies in the core were calculated. The pitch size of whole hexagon assemblies was increase by 0.5% and 1.0% compared to its original size (13.636 cm) to evaluate the reactivity change in uniform core expansion cases.

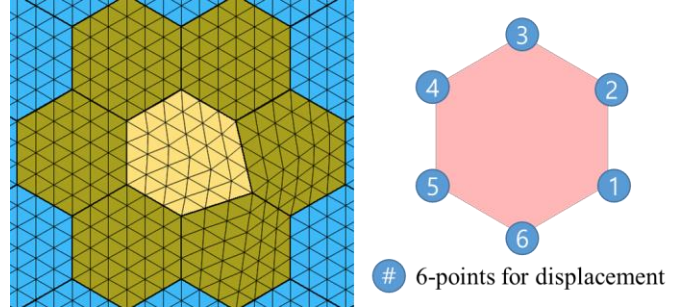


Fig. 5. Example of Hexagon Assembly Deformation (Left) and 6-vertices for Node Displacement (Right)

In the case of irregular deformation of assemblies, two types of deformation were considered depending on whether regular uniform expansion by 0.5% of pitch size is applied or not before irregular deformation. To imitate the irregular deformations, an arbitrary vertex among six vertices of a hexagon assembly was randomly moved. During a junction point movement between assemblies, the total number of triangular elements in the problem domain was not changed. An example of the irregular deformation via the junction point movement is depicted in Fig. 5. 9-group constants were properly weighted by the volume ratio for both the regular and irregular deformation cases.

The ranges of random displacement of vertices for three types of irregular deformation scenarios are listed as below:

- (1) 0.1~0.5% of pitch size without any uniform expansion.
- (2) 0.5~7.0% of pitch size without any uniform expansion.
- (3) 0.05~0.25% of pitch size after 0.5% regular uniform expansion.

The ranges were chosen so that the maximum displacement would be less than 1 cm. The irregular deformation scenarios (1) ~ (3) are named as 'Mixed Expansion (1) ~ (3)' in section III.

III. NUMERICAL RESULTS

1. Reference Calculation using MCNP5

As already mentioned in Section II, the reference results were calculated by using MCNP5. The input files for MCNP5 calculations are automatically generated by the FEM mesh generator so that the same geometry can be transferred to MCNP surface card decks regardless of geometric perturbations. To avoid complicated processing for surface card generation via considering all triangular elements in the problem domain, only the node information for 6 vertices in hexagonal assemblies is utilized to generate surface card decks in MCNP5. Figure 6 shows the PGSFR geometry from the mesh generator plotter and MCNP5 plotter.

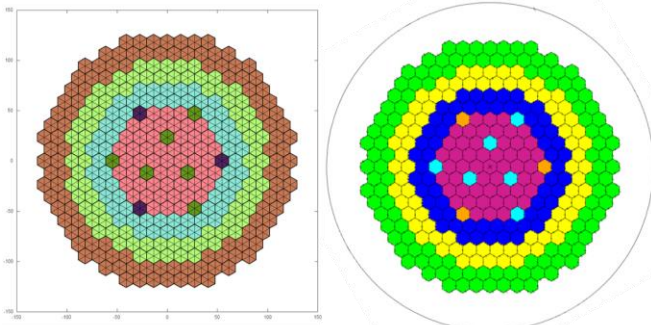


Fig. 6. Geometry Plotting by using Mesh Generator (Left) and MCNP5 Plot Function (Right)

Instead of using the ENDF library, the same 9-group cross sections which were used in FEM-based diffusion analysis were also used in MCNP5 calculation with the intrinsic multi-group option.

In order to obtain a precise standard deviation less than 1 pcm in Monte Carlo simulation, 2,000,000 particles per cycle with a total of 5,000 cycles (500 inactive) were used. All the MCNP5 calculations were performed with 84 cores per simulation. The reference results for whole deformation scenarios are summarized in Table I.

Table I. Reference Reactivity Change due to Assembly Deformation

Event	MCNP5 ($1\sigma \approx \pm 0.6 \text{ pcm}$)		
	Time (sec)	k-eff	$\Delta\rho$ (pcm)
Original	718,387	1.284491	-
Uniform Expan. (1)	1,020,678	1.283222	-76.998
Uniform Expan. (2)	994,549	1.281929	-155.629
Mixed Expan. (1)	993,646	1.284487	-0.279
Mixed Expan. (2)	1,021,103	1.284436	-3.386
Mixed Expan. (3)	979,339	1.283213	-77.549

Original: without any expansion or deformation
 Uniform Expan. (1): 0.5% Uniform expansion
 Uniform Expan. (2): 1.0% Uniform expansion
 Mixed Expan. (1): 0.0% Uniform expansion + 0.10~0.50% Irregular deformation randomly
 Mixed Expan. (2): 0.0% Uniform expansion + 0.50~7.00% Irregular deformation randomly
 Mixed Expan. (3): 0.5% Uniform expansion + 0.05~0.25% Irregular deformation randomly

2. A Comparison of FEM Results with MCNP5 Results

For the given deformation scenarios, FEM-based estimation of reactivity changes was conducted and was compared to that of the reference calculated by MCNP5. The accuracy of the finite element analysis is generally affected by the mesh refinement. Therefore, the dependency

of the reactivity change estimation in fast reactor analysis on the mesh refinement was also assessed. The indicator for mesh refinement is the number of division on the one side of the hexagon assembly. If the number of sub-sides per single side of hexagon increases, the total number of triangular elements in a single hexagon will increase. For easier understanding, two example of mesh refinement depending on the number of sub-sides is shown in Fig. 7.

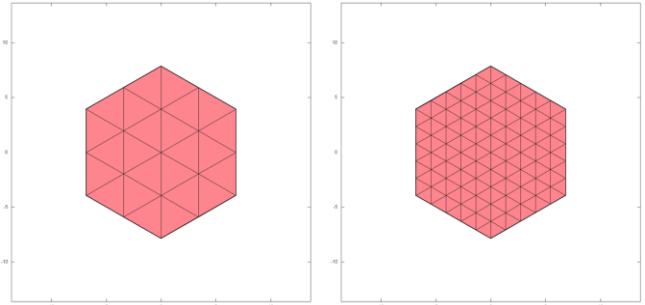


Fig. 7. Examples for mesh refinement per hexagon assembly, 2 sub-sides (Left) and 5 sub-sides (Right)

The k-effs depending on the mesh refinement is shown in Fig. 8. It is clearly seen that k-effs converge in division number 5~7 as increasing the order of mesh refinement.

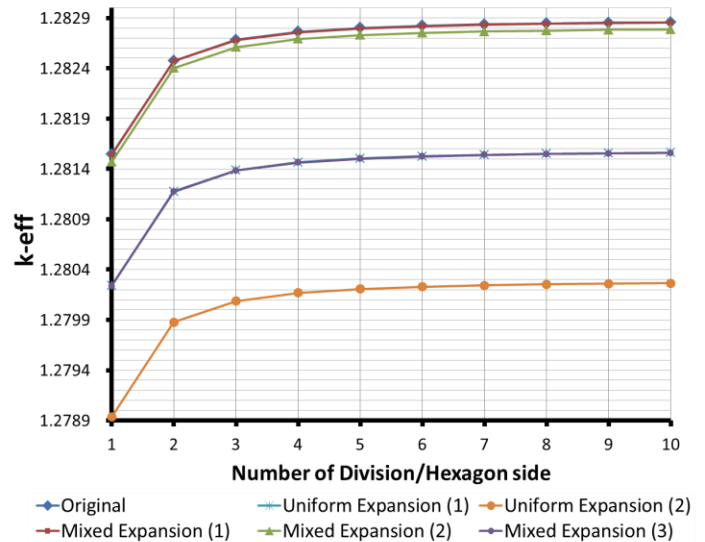


Fig. 8. k-eff depending on the mesh refinement

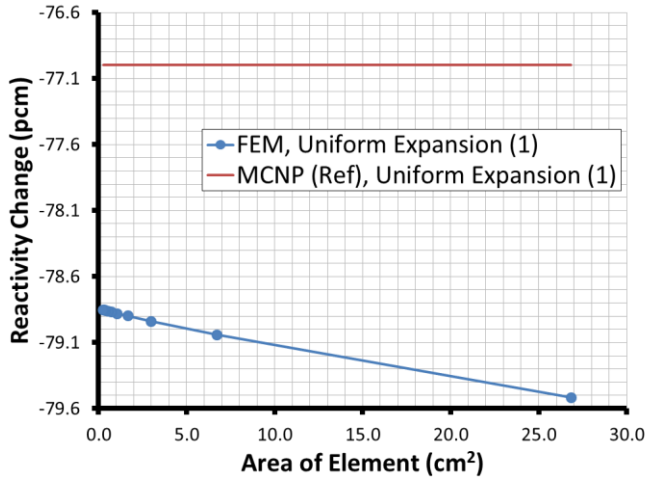


Fig. 9. Reactivity Change depending on Area of Triangular Element in Uniform Expansion (1)

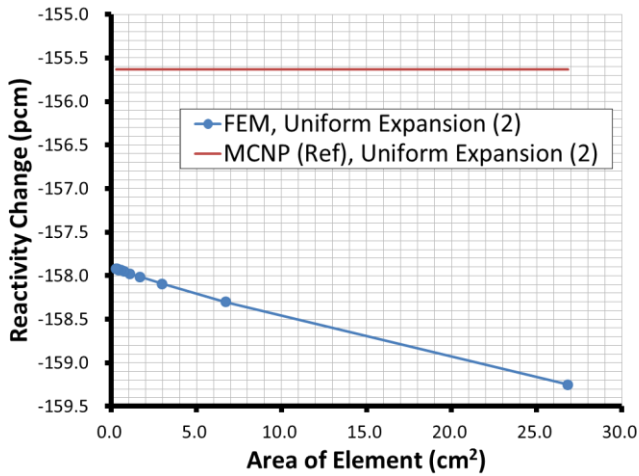


Fig. 10. Reactivity Change depending on Area of Triangular Element in Uniform Expansion (2)

The reactivity changes depending on the area of the triangular element are plotted in Fig. 9 and 10 for uniform expansion scenario (1) and (2), respectively. As expected, it is shown that the reactivity changes are approaching the reference as the area of the triangular element becomes smaller and smaller.

The reactivity changes from FEM calculation is summarized in Table II and III for each assembly deformation scenario. Similarly to the k-eff convergence, the reactivity changes also begin to converge when the division number per side is greater than 4. It is shown that the FEM estimations match quite well with the MCNP results with a maximum difference of ~2.5 pcm for a large perturbation. This means that the FEM-based diffusion analysis with low-order approximation has high feasibility to estimate the reactivity changes caused by geometric perturbations in fast reactors via error cancellation. Based on the current results, it is expected that if the error from the geometric perturbation is not very big, most of the errors in

diffusion analysis can be successfully removed in the estimation of the deformation-related reactivity changes.

Table II. Evaluated Reactivity Change due to Assembly Deformation Scenarios: Uniform Expansions

# of Division	Event		
	k-eff, Original	$\Delta\rho$ (pcm), Uniform Expan. (1)	$\Delta\rho$ (pcm), Uniform Expan. (2)
Ref.	1.284491	-76.998	-155.629
1	1.2815445	-79.516	-159.249
2	1.2824752	-79.042	-158.301
3	1.2826832	-78.939	-158.093
4	1.2827628	-78.899	-158.013
5	1.2828018	-78.881	-157.977
6	1.2828237	-78.869	-157.953
7	1.2828373	-78.861	-157.936
8	1.2828464	-78.859	-157.934
9	1.2828527	-78.852	-157.923
10	1.2828573	-78.853	-157.920

Table III. Evaluated Reactivity Change due to Assembly Deformation Scenarios: Mixed Expansions

# of Division	Event		
	$\Delta\rho$ (pcm), Mixed Expan. (1)	$\Delta\rho$ (pcm), Mixed Expan. (2)	$\Delta\rho$ (pcm), Mixed Expan. (3)
Ref.	-0.279	-3.386	-77.549
1	-0.291	-4.624	-79.657
2	-0.286	-4.433	-79.180
3	-0.285	-4.385	-79.076
4	-0.283	-4.363	-79.035
5	-0.284	-4.354	-79.017
6	-0.282	-4.346	-79.004
7	-0.281	-4.341	-78.996
8	-0.284	-4.342	-78.995
9	-0.280	-4.336	-78.988
10	-0.281	-4.333	-78.987

IV. CONCLUSIONS

In this study, the estimation of reactivity changes due to the assembly deformations was conducted with a newly-developed FEM method for a 2-D SFR core. For 5 types of core deformation scenarios, the reactivity changes were calculated by using the FEM-based diffusion analysis and the results were compared with Monte Carlo simulations. The results show that the FEM-based diffusion analysis with low-order approximation can well predict the reactivity

change due to the geometric perturbation in SFRs. We found that prediction error of the FEM-based diffusion method is less than ~-2.5 pcm for all deformation scenarios. Actual geometrical deformations will be considered for 3D geometry in the future work.

APPENDIX A: 9-GROUP CROSS SECTIONS USED IN PGSFR ANALYSIS (BEFORE PERTURBATION)

Inner Core FA				
Group	D	Absorption	Nu-fission	Fission Spectrum
1	1.956E+00	7.007E-03	4.121E-02	2.578E-02
2	1.829E+00	7.969E-03	1.981E-02	5.580E-01
3	1.692E+00	4.218E-03	6.846E-03	2.898E-01
4	1.421E+00	4.602E-03	7.091E-03	9.542E-02
5	1.238E+00	6.207E-03	8.532E-03	2.381E-02
6	9.739E-01	9.295E-03	1.056E-02	5.515E-03
7	1.146E+00	1.282E-02	1.387E-02	1.302E-03
8	6.368E-01	1.883E-02	2.030E-02	2.871E-04
9	6.479E-01	3.996E-02	4.559E-02	9.014E-05

Group Scattering Matrix			
Group	1	2	3
1	9.656E-02	3.601E-02	1.950E-02
2	0.000E+00	1.303E-01	2.918E-02
3	0.000E+00	0.000E+00	1.739E-01
4	0.000E+00	0.000E+00	0.000E+00
5	0.000E+00	0.000E+00	0.000E+00
6	0.000E+00	0.000E+00	0.000E+00
7	0.000E+00	0.000E+00	0.000E+00
8	0.000E+00	0.000E+00	0.000E+00
9	0.000E+00	0.000E+00	0.000E+00
Group	4	5	6
1	8.410E-03	2.270E-03	5.183E-04
2	1.162E-02	2.598E-03	4.614E-04
3	1.598E-02	2.303E-03	4.458E-04
4	2.205E-01	9.343E-03	1.132E-04
5	0.000E+00	2.557E-01	7.253E-03
6	0.000E+00	0.000E+00	3.246E-01
7	0.000E+00	0.000E+00	0.000E+00
8	0.000E+00	0.000E+00	0.000E+00
9	0.000E+00	0.000E+00	0.000E+00
Group	7	8	9
1	1.117E-04	2.650E-05	1.020E-05
2	8.705E-05	1.809E-05	5.638E-06
3	1.184E-04	3.972E-05	7.425E-06
4	1.499E-05	1.842E-06	3.046E-07
5	1.506E-04	8.219E-06	1.648E-06
6	8.222E-03	1.275E-04	2.515E-05
7	2.735E-01	4.600E-03	2.290E-05
8	0.000E+00	4.938E-01	1.079E-02
9	0.000E+00	0.000E+00	4.745E-01

Outer Core FA				
Group	D	Absorption	Nu-fission	Fission Spectrum
1	1.956E+00	7.006E-03	4.121E-02	2.577E-02
2	1.829E+00	7.972E-03	1.982E-02	5.581E-01
3	1.692E+00	4.218E-03	6.844E-03	2.898E-01
4	1.422E+00	4.602E-03	7.091E-03	9.540E-02

5	1.238E+00	6.215E-03	8.537E-03	2.380E-02
6	9.784E-01	9.295E-03	1.057E-02	5.512E-03
7	1.146E+00	1.282E-02	1.387E-02	1.301E-03
8	6.372E-01	1.894E-02	2.048E-02	2.869E-04
9	6.624E-01	4.576E-02	5.357E-02	9.000E-05

Group Scattering Matrix			
Group	1	2	3
1	9.656E-02	3.601E-02	1.950E-02
2	0.000E+00	1.304E-01	2.915E-02
3	0.000E+00	0.000E+00	1.740E-01
4	0.000E+00	0.000E+00	0.000E+00
5	0.000E+00	0.000E+00	0.000E+00
6	0.000E+00	0.000E+00	0.000E+00
7	0.000E+00	0.000E+00	0.000E+00
8	0.000E+00	0.000E+00	0.000E+00
9	0.000E+00	0.000E+00	0.000E+00
Group	4	5	6
1	8.410E-03	2.270E-03	5.183E-04
2	1.161E-02	2.598E-03	4.612E-04
3	1.585E-02	2.299E-03	4.449E-04
4	2.205E-01	9.240E-03	1.127E-04
5	0.000E+00	2.555E-01	7.416E-03
6	0.000E+00	0.000E+00	3.226E-01
7	0.000E+00	0.000E+00	0.000E+00
8	0.000E+00	0.000E+00	0.000E+00
9	0.000E+00	0.000E+00	0.000E+00
Group	7	8	9
1	1.117E-04	2.650E-05	1.020E-05
2	8.701E-05	1.808E-05	5.637E-06
3	1.182E-04	3.959E-05	7.407E-06
4	1.491E-05	1.838E-06	3.042E-07
5	1.537E-04	8.175E-06	1.651E-06
6	8.637E-03	1.285E-04	2.531E-05
7	2.734E-01	4.590E-03	2.274E-05
8	0.000E+00	4.915E-01	1.267E-02
9	0.000E+00	0.000E+00	4.574E-01

Reflector			
Group	D	Absorption	Nu-fission
1	1.372E+00	5.247E-03	-
2	1.525E+00	4.062E-04	-
3	1.848E+00	2.754E-04	-
4	1.698E+00	2.717E-04	-
5	1.472E+00	4.084E-04	-
6	8.619E-01	5.071E-04	-
7	1.382E+00	4.145E-04	-
8	4.082E-01	1.115E-03	-
9	4.812E-01	4.414E-03	-

Group Scattering Matrix			
Group	1	2	3
1	1.395E-01	7.075E-02	2.075E-02
2	0.000E+00	1.689E-01	4.310E-02
3	0.000E+00	0.000E+00	1.623E-01
4	0.000E+00	0.000E+00	0.000E+00
5	0.000E+00	0.000E+00	0.000E+00
6	0.000E+00	0.000E+00	0.000E+00
7	0.000E+00	0.000E+00	0.000E+00
8	0.000E+00	0.000E+00	0.000E+00

9	0.000E+00	0.000E+00	0.000E+00
Group	4	5	6
1	5.128E-03	1.227E-03	3.001E-04
2	4.746E-03	1.049E-03	2.782E-04
3	1.552E-02	1.678E-03	3.320E-04
4	1.874E-01	8.679E-03	1.451E-05
5	0.000E+00	2.175E-01	8.549E-03
6	0.000E+00	0.000E+00	3.726E-01
7	0.000E+00	0.000E+00	0.000E+00
8	0.000E+00	0.000E+00	0.000E+00
9	0.000E+00	0.000E+00	0.000E+00
Group	7	8	9
1	6.361E-05	2.217E-05	1.280E-05
2	5.156E-05	9.287E-06	2.688E-06
3	1.867E-04	8.905E-05	1.116E-05
4	1.512E-06	2.959E-07	4.858E-08
5	2.494E-06	5.019E-07	1.019E-07
6	1.366E-02	0.000E+00	0.000E+00
7	2.303E-01	1.041E-02	7.242E-05
8	0.000E+00	7.857E-01	2.985E-02
9	0.000E+00	0.000E+00	6.883E-01

B4C Shield			
Group	D	Absorption	Nu-fission
1	1.945E+00	4.165E-03	-
2	1.555E+00	5.122E-03	-
3	1.367E+00	6.454E-03	-
4	9.616E-01	1.544E-02	-
5	8.749E-01	2.626E-02	-
6	7.005E-01	4.005E-02	-
7	7.465E-01	6.436E-02	-
8	4.982E-01	1.053E-01	-
9	3.691E-01	3.022E-01	-
Group Scattering Matrix			
Group	1	2	3
1	8.837E-02	6.293E-02	1.088E-02
2	0.000E+00	1.432E-01	6.363E-02
3	0.000E+00	0.000E+00	1.755E-01
4	0.000E+00	0.000E+00	0.000E+00
5	0.000E+00	0.000E+00	0.000E+00
6	0.000E+00	0.000E+00	0.000E+00
7	0.000E+00	0.000E+00	0.000E+00
8	0.000E+00	0.000E+00	0.000E+00
9	0.000E+00	0.000E+00	0.000E+00
Group	4	5	6
1	2.173E-03	4.610E-04	1.074E-04
2	1.400E-03	3.125E-04	8.534E-05
3	6.107E-02	6.141E-04	1.056E-04
4	2.743E-01	5.693E-02	5.485E-06
5	0.000E+00	3.021E-01	5.266E-02
6	0.000E+00	0.000E+00	3.870E-01
7	0.000E+00	0.000E+00	0.000E+00
8	0.000E+00	0.000E+00	0.000E+00
9	0.000E+00	0.000E+00	0.000E+00
Group	7	8	9
1	2.271E-05	7.252E-06	3.881E-06
2	1.579E-05	2.741E-06	7.320E-07
3	5.819E-05	2.777E-05	3.472E-06

4	6.418E-07	9.871E-08	1.658E-08
5	8.139E-07	1.358E-07	2.423E-08
6	4.886E-02	0.000E+00	0.000E+00
7	3.447E-01	3.738E-02	2.380E-05
8	0.000E+00	5.281E-01	3.565E-02
9	0.000E+00	0.000E+00	6.007E-01

Primary CA (Unrodded)			
Group	D	Absorption	Nu-fission
1	5.584E+00	1.867E-03	-
2	4.449E+00	6.277E-05	-
3	3.154E+00	3.609E-05	-
4	3.376E+00	4.750E-05	-
5	3.407E+00	6.305E-05	-
6	2.434E+00	9.155E-05	-
7	2.943E+00	5.176E-05	-
8	1.167E+00	1.767E-04	-
9	1.727E+00	8.793E-04	-
Group Scattering Matrix			
Group	1	2	3
1	2.830E-02	2.374E-02	4.540E-03
2	0.000E+00	6.139E-02	1.227E-02
3	0.000E+00	0.000E+00	9.327E-02
4	0.000E+00	0.000E+00	0.000E+00
5	0.000E+00	0.000E+00	0.000E+00
6	0.000E+00	0.000E+00	0.000E+00
7	0.000E+00	0.000E+00	0.000E+00
8	0.000E+00	0.000E+00	0.000E+00
9	0.000E+00	0.000E+00	0.000E+00
Group	4	5	6
1	9.897E-04	2.047E-04	4.633E-05
2	9.373E-04	1.967E-04	4.733E-05
3	1.138E-02	8.935E-04	6.274E-05
4	9.137E-02	7.312E-03	1.009E-05
5	0.000E+00	9.132E-02	6.458E-03
6	0.000E+00	0.000E+00	1.282E-01
7	0.000E+00	0.000E+00	0.000E+00
8	0.000E+00	0.000E+00	0.000E+00
9	0.000E+00	0.000E+00	0.000E+00
Group	7	8	9
1	9.357E-06	2.663E-06	1.379E-06
2	8.986E-06	1.609E-06	4.544E-07
3	2.128E-05	1.015E-05	1.275E-06
4	3.533E-06	4.074E-07	7.082E-08
5	3.268E-07	5.297E-08	9.425E-09
6	8.676E-03	0.000E+00	0.000E+00
7	1.080E-01	5.257E-03	8.052E-06
8	0.000E+00	2.599E-01	2.545E-02
9	0.000E+00	0.000E+00	1.921E-01

Secondary CA (Unrodded)			
Group	D	Absorption	Nu-fission
1	5.584E+00	1.867E-03	-
2	4.450E+00	6.366E-05	-
3	3.144E+00	3.615E-05	-
4	3.375E+00	4.746E-05	-
5	3.408E+00	6.307E-05	-
6	2.445E+00	9.094E-05	-

7	2.949E+00	5.202E-05	-
8	1.149E+00	1.784E-04	-
9	1.683E+00	8.807E-04	-
Group Scattering Matrix			
Group	1	2	3
1	2.830E-02	2.374E-02	4.540E-03
2	0.000E+00	6.148E-02	1.216E-02
3	0.000E+00	0.000E+00	9.382E-02
4	0.000E+00	0.000E+00	0.000E+00
5	0.000E+00	0.000E+00	0.000E+00
6	0.000E+00	0.000E+00	0.000E+00
7	0.000E+00	0.000E+00	0.000E+00
8	0.000E+00	0.000E+00	0.000E+00
9	0.000E+00	0.000E+00	0.000E+00
Group	4	5	6
1	9.897E-04	2.047E-04	4.633E-05
2	9.444E-04	1.979E-04	4.743E-05
3	1.120E-02	8.964E-04	6.217E-05
4	9.150E-02	7.201E-03	1.012E-05
5	0.000E+00	9.122E-02	6.515E-03
6	0.000E+00	0.000E+00	1.273E-01
7	0.000E+00	0.000E+00	0.000E+00
8	0.000E+00	0.000E+00	0.000E+00
9	0.000E+00	0.000E+00	0.000E+00
Group	7	8	9
1	9.357E-06	2.663E-06	1.379E-06
2	9.001E-06	1.615E-06	4.577E-07
3	2.138E-05	1.020E-05	1.281E-06
4	3.547E-06	4.091E-07	7.111E-08
5	3.226E-07	5.299E-08	9.532E-09
6	8.983E-03	0.000E+00	0.000E+00
7	1.078E-01	5.111E-03	7.990E-06
8	0.000E+00	2.615E-01	2.855E-02
9	0.000E+00	0.000E+00	1.972E-01

NOMENCLATURE

k_{eff} = Effective multiplication factor

ϕ_g = g^{th} -group flux

$\eta_{i,j,k}^e$ = Shape function at i -, j -, k -node

e = sub-domain

i, j, k = nodes in a sub-domain

D_g = g^{th} -group diffusion coefficient

Σ_{rg} = g^{th} -group removal cross section

$\Sigma_{sg' \rightarrow g}$ = g'^{th} -group to g^{th} -group cross section

$\nu\Sigma_{fg}$ = g^{th} -group nu-fission cross section

γ = Boundary condition

Γ_e = Surface length of sub-domain e

ACKNOWLEDGMENTS

This work was supported by the National Research Foundation of Korea (NRF) Grant funded by the Korean Government (MSIP) (NRF-2016R1A5A1013919).

REFERENCES

1. D. C. WADE and Y. I. CHAN, "The integral fast reactor (IFR) concept: Physics of operation and safety," *Nuclear Science and Engineering*, Vol. 100, p. 507-524 (1988).
2. MARK REED, Kord Smith, and Benoit Forget, "The Virtual Density Theory of Neutronics: A Generic Method for Geometry Distortion Reactivity Coefficients," *Proc. PHYSOR 2014*, Kyoto, Japan, Sep. 28-Oct. 3, 2014 (2014) (CD-ROM).
3. KOREA ATOMIC ENERGY RESEARCH INSTITUTE and SODIUM-COOLED FAST REACTOR DEVELOPMENT AGENCY, "The 3rd International Technical Review Meeting for Prototype Gen IV SFR (PGSFR) Development in Korea," compiled files (2014)
4. R. E. MACFARLANE, "TRANSX 2: A Code for Interfacing MATXS Cross-Section Libraries to Nuclear Transport Codes," LA-12312-MS (1992).
5. R. E. ALCOUFFE, et al., "DANTSYS: A Diffusion Accelerated Neutral Particle Transport Code System," LA-12969-M (1995).
6. X-5 MONTE CARLO TEAM, "MCNP: A General Monte Carlo N-Particle Transport Code, Version 5," Los Alamos National Laboratory (2003).